Photosynthesis Research manuscript No.
(will be inserted by the editor)

The role of Charge Transfer states in the spectral tuning of antenna complexes of purple bacteria.

Michele Nottoli[1] · **Sandro Jurinovich**[1] · **Lorenzo Cupellini**[1] · **Alastair T. Gardiner**[2] · **Richard Cogdell**[2] · **Benedetta Mennucci**[1]

Abstract The LH2 antenna complexes of purple bacteria occur, depending on light conditions, in various different spectroscopic forms, with a similar structure but different absorption spectra. The differences are related to point changes in the primary amino acid sequence, but the molecular-level relationship between these changes and the resulting spectrum is still not well understood. We undertook a systematic quantum chemical analysis of all the main factors that contribute to the exciton structure, looking at how the environment modulates site energies and couplings in the B800-850 and B800-820 spectroscopic forms of LH2. A multiscale approach combining quantum chemistry and an atomistic classical embedding has been used where mutual polarization effects between the two parts are taken into account. We find that the loss of hydrogen bonds following amino acid changes can only explain a part of the observed blue shift in the B850 band. The coupling of excitonic states to charge transfer states, which is different in the two forms, contributes with a similar amount to the overall blue shift.

1 Introduction

The typical photosynthetic unit (PSU) found in purple photosynthetic bacteria contains two types of light harvesting complexes, LH1/RC core complexes and LH2 complexes [1,2]. The composition of the PSU and its size are not fixed. Rather they are regulated by a variety of environmental conditions, such as light intensity [3,4]. Moreover, when some species, such as *Rps. acidophila*, are grown at low light intensity they also change the spectroscopic form of the LH2 complex that is synthesised [5,6]. This ability to change the type of LH2 complex in response to growth at different light intensities is found in species that have a multigene family of the pucBA genes that encode the LH2 apoproteins [7]. When *Rps. acidophila* is grown at high light it produces the well-known B800-850 form of LH2, while when

[1] Dipartimento di Chimica e Chimica Industriale, University of Pisa, Via G. Moruzzi 13, I-56124 Pisa, Italy E-mail: benedetta.mennucci@unipi.it
[2] Glasgow Biomedical Research Centre, Institute of Molecular Cell and Systems Biology, University of Glasgow, 126 University Place, Glasgow, G12 8TA

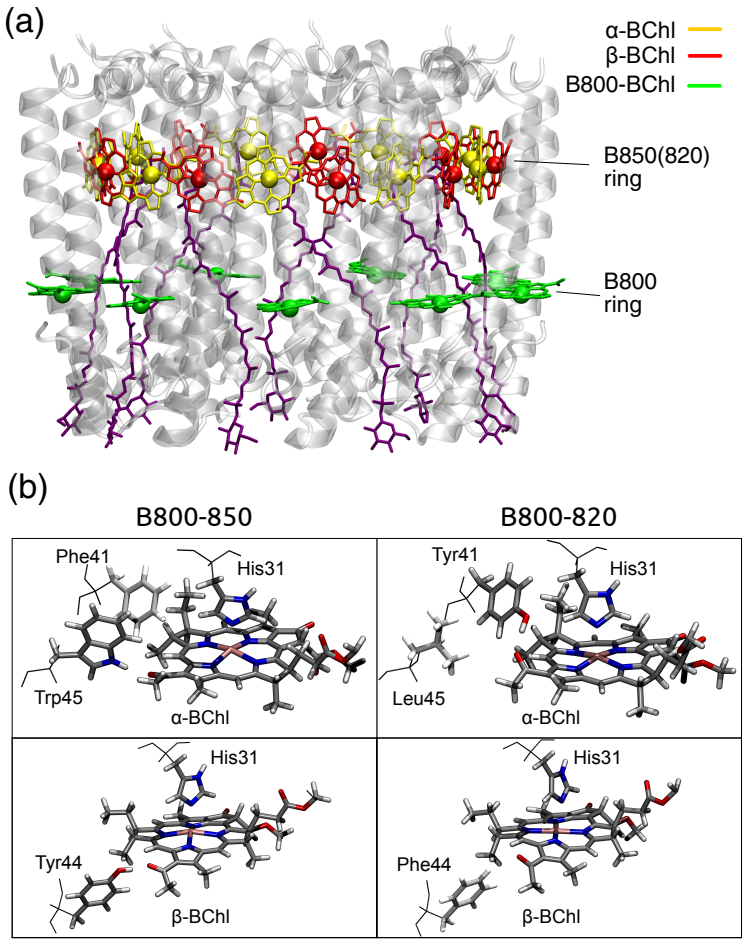

Fig. 1 (a) LH2 of Rps. acidophila LH2 is a cylindrical complex containing nine identical subunits. Each subunit is constituted by a pair of $\alpha\beta$-apoproteins, which binds three BChls a. The BChls are organized into two rings: the B800 ring, in which 9 BChls are arranged perpendicular to the cylinder axis, and the B850 ring, in which 18 BChls are oriented with their plane parallel to the cylinder axis. The B850 BChls are named α or β depending on the apoprotein that binds the central Mg. The nine carotenoid molecules bound by LH2 are also shown in purple. (b) Graphical representation of the hydrogen-bond network involving BChls in LH2 and LH3. Axial ligands are also shown.

it is grown at low light it makes the B800-820 form of LH2 (which is sometimes denoted as LH3 in the literature) [5]. The names are related to the characteristic near-infrared absorption spectrum of each LH2, which is composed of two bands, at 800 and 850 nm or 820 nm, respectively: these peaks arise from the contribution of the bright (Q_y) transitions of the embedded Bacteriochlorophylls a (BChl) arranged in two rings as shown in Fig. 1.

Sequencing the α and β apoproteins of the two spectroscopic forms of LH2 revealed that the shift of the 850 nm absorption band to 820 nm was correlated with two changes in the amino acid sequence in the C-terminal region of the α

apoprotein at positions α 44 and 45 [8]. In B800-850 these two amino acids are tyrosine and tryptophan while in B800-820 they are phenylalanine and leucine respectively (see Fig. 1b). Site-directed mutagenesis [9] has been used to introduce equivalent changes into the α apoprotein of the LH2 complex from *Rhodobacter sphaeroides*. These changes caused the B850 band of the *Rb. sphaeroides* to shift to 820 nm. Resonance Raman spectroscopy showed that this shift of the absorption spectrum from 850 to 820 nm was accompanied by a loss of hydrogen bonding to the strongly coupled B850 BChls [10]. Later an X-ray crystal structure was obtained for the B800-820 complex from *Rps. acidophila* [11]. A comparison of the structure of this form of LH2 with the previously determined structure of the B800-850 form of LH2 revealed the expected change in hydrogen bonding. The loss of the two hydrogen bonds also results in a rotation of an acetyl group with respect to the plane of the bacteriochlorin ring. Such a rotation has the effect of reducing the extent of the degree of conjugation in the bacteriochlorin rings and to change that BChl's site energy, moving it to the blue [12]. Therefore it was suggested that the blue shift of the absorption from 850 to 820 nm was due to this change in site energy resulting from the reduction in conjugation. However, it has recently been questioned as to whether this effect of change in the length of conjugation is large enough to account for the full wavelength shift from 850 to 820 nm [13]. Moreover, spectroscopic studies have suggested that the electronic couplings are reduced in B800-B820 with respect to those of LH2 [14, 13]. However, there is still no clear picture of how the changes in primary structure of the apoproteins on going from B800-850 to B850-820 affect the spectral properties of the complex.

Recently, experimental evidence has suggested that charge transfer (CT) states influence the spectral properties of LH2 [15]. Theoretical calculations have also shown that charge-transfer configurations have a significant effect on the exciton energies [16, 17]. The change in hydrogen bonding in the B850-B820 form of LH2 could affect the energies of these CT states and the extent of their mixing with exciton states. For this reason, CT states should also be accounted for when comparing the two forms of LH2.

In the present work we used quantum chemical simulations based on an excitonic approach [18] and applied them to the two crystal structures of the B800-850 and B800-820 forms of LH2 to understand the molecular origin of their spectral differences. We carried out a systematic analysis of the interactions between BChls and the protein matrix and their effect on site energies and couplings. We employed a multiscale polarizable quantum mechanics/molecular mechanics (QM/MMPol) method [19], able to describe all the main intermolecular interactions that tune the Q_y excitation energies of BChls, as well as the direct and indirect influence of the protein on the electronic couplings. In order to assess the effect of charge transfer states on the exciton structure we extended the excitonic model to include all CT states between adjacent B850(B820) BChls. The CT states are allowed to mix with the Q_y states of the BChls, influencing the exciton structure of the system.

Our results confirm that the site energies of the β-BChl in the B800-B820 complex are influenced by the loss of hydrogen bonding; however, only small differences were found for the α-BChl site energy and for the electronic couplings. These changes alone, therefore, cannot explain the large blue shift experienced by the B850 band in the B800-B820 form. A significant role is played by the CT states. The inclusion of CT states in the excitonic Hamiltonian enhances the differences

between the two complexes improving the agreement between the simulated and experimental spectra.

2 Methods

2.1 Excitonic states

By assuming that each BChl contributes to the excited state manifold of the LH2 complexes through a single (Q_y) excitation, the excitonic Hamiltonian reads:

$$\hat{H}_{ex} = \sum_{i}^{27} \mathcal{E}_i \left|i\right\rangle \left\langle i\right| + \sum_{ij}^{27} V_{ij} \left|i\right\rangle \left\langle j\right| \tag{1}$$

where $\mathcal{E}_i$ is the Q_y excitation energy (site energy) of each BChl (27 in total) and V_{ij} is the electronic coupling between two excitations of different BChls. The resulting exciton energies, and the relative composition in terms of the localized states, are obtained by diagonalization of $\hat{H}_{ex}$. The excitonic analysis was carried out using our EXAT program [20].

In order to include charge-transfer (CT) states between the 18 BChls in the B850 (or B820) ring, we have to extend the Hamiltonian of eq. 1 with the CT excitation energies $\mathcal{E}_m^{CT}$ and the couplings V_{im}^{CT-Qy} between CT and Q_y states.

$$\hat{H}_{ex-CT} = \hat{H}_{ex} + \sum_{m}^{36} \mathcal{E}_m^{CT} \left|m\right\rangle \left\langle m\right| + \sum_{i}^{18} \sum_{m}^{36} \left(V_{im}^{CT-Qy} \left|i\right\rangle \left\langle m\right| + h.c. \right) \tag{2}$$

where the index i runs on the Q_y excited states only, whereas index m runs on the CT states. For every $\alpha\beta$ pair of adjacent BChls in the B850 (or 820) ring, there are two distinct CT states, namely $\alpha \rightarrow \beta$ (where one electron moves from the α-BChl to the β-BChl) and $\beta \rightarrow \alpha$ (where the electron moves from the β-BChl to the α-BChl), summing to a total of 36 CT states. The Q_y excited state (α^* or β^*) of any BChl α or β is only coupled to those CT states that involve the same pigment. For each $\alpha\beta$ pair of BChls there are four possible couplings involving CT states, namely, $V_{\alpha^*,\alpha\rightarrow\beta}$, $V_{\beta^*,\alpha\rightarrow\beta}$, $V_{\alpha^*,\beta\rightarrow\alpha}$, and $V_{\beta^*,\beta\rightarrow\alpha}$. We separately computed the couplings to CT states for the two possible $\alpha\beta$ BChl pairs, namely the intra-dimer and for the inter-dimer BChl pairs (See Figure S3 in the Supporting Information).

Q_y energies and couplings. The elements of the exciton Hamiltonian $\hat{H}_{ex}$ were computed using the QM/MMPol multiscale method. Briefly, the QM/MMPol embedding treats the BChl of interest at the QM level, whereas the rest of the system is treated classically as a set of point charges and induced dipoles [19]. The environment is allowed to polarize in response to the QM density, in turn creating a field that acts back on the QM part. The presence of the polarizable embedding allows to describe the effect of the atomistic environment of the protein on the site energies and transition densities of the pigments.

The electronic couplings are computed with a well established method based on the transition densities of the interacting pigments [21, 22, 19]. Considering only

the Coulomb part, the coupling between two molecules i and j reads:

$$V_{ij} = \int \mathrm{d}\mathbf{r} \int \mathrm{d}\mathbf{r}' \, \frac{\rho_i^{tr}(\mathbf{r}')\rho_j^{tr}(\mathbf{r})}{|\mathbf{r}-\mathbf{r}'|} - \sum_k \left(\int \mathrm{d}\mathbf{r} \, \rho_i^{tr}(\mathbf{r}) \frac{\mathbf{r}_k - \mathbf{r}}{|\mathbf{r}_k - \mathbf{r}|^3} \right) \boldsymbol{\mu}_k^{ind}(\rho_j^{tr}) \qquad (3)$$

where ρ_i^{tr} and ρ_j^{tr} are the transition densities of i and j, the summation runs on the polarizable atoms of the environment, and $\boldsymbol{\mu}_k^{ind}$ is the dipole induced on atom k by the field generated by ρ_j^{tr}. The first and second term of eq. 3 represent the bare Coulomb coupling V_{Coul} and the explicit environment-mediated coupling in the MMPol formulation V_{MMPol}.

2.2 CT energies and couplings.

The couplings between CT and Q_y states were determined using a diabatization scheme that combines the Fragment Charge Difference (FCD) [23,24] and Fragment Excitation Difference (FED) [25] methods, starting from a calculation on the dimeric target system. In the present case, the excited states of a BChl dimer are combinations of Q_y states (such as $\alpha\beta^*$ and $\alpha^*\beta$), other locally excited (LE) states, and CT states (such as $\alpha^-\beta^+$ and $\alpha^+\beta^-$).

FED and FCD methods. Let us consider a dimer composed of two molecules A and B. The FED scheme can recover the diabatic (localized) basis from delocalized excited states by using an additional operator Δx, which measures the difference in excitation number between A and B. The elements of the Δx matrix are defined as:[25]

$$\Delta x_{mn} = \int_{\mathbf{r}\in B} \rho_{mn}^{\mathrm{ex}}(\mathbf{r})\mathrm{d}\mathbf{r} - \int_{\mathbf{r}\in A} \rho_{mn}^{\mathrm{ex}}(\mathbf{r})\mathrm{d}\mathbf{r} \qquad (4)$$

where ρ_{mn}^{ex} is the excitation density, defined within CIS as:[25]

$$\rho_{mn}^{\mathrm{ex}}(\mathbf{r}) = \sum_{ij}\sum_a t_{ia}^{(m)} t_{ja}^{(n)*} \phi_i(\mathbf{r})\phi_j^*(\mathbf{r}) + \sum_i \sum_{ab} t_{ia}^{(m)} t_{ib}^{(n)*} \phi_a(\mathbf{r})\phi_b^*(\mathbf{r}) \qquad (5)$$

and $t_{ia}^{(m)}$ are the CIS coefficients of state m; i,j represent occupied molecular orbitals, and a,b represent virtual molecular orbitals. The quantity Δx has its extrema when the excitation is entirely localized on either A or B. If the states m and n are the combination of two states, AB^* localized on B, and A^*B localized on A, the eigenvectors of the 2×2 Δx matrix represent the transformation from the adiabatic to the diabatic basis ($\mathbb{U}$), and the eigenvalues are either 1 or -1 for AB^* and A^*B.[25] The diagonal matrix of adiabatic energies can be transformed into the diabatic basis of AB^* and A^*B, and the electronic coupling between these states is found as the off-diagonal element.

The same strategy can be applied to computing the coupling to CT states, using the FCD method with the additional operator Δq to localize the electronic charge:[23]

$$2\Delta q_{nm} = \int_{\mathbf{r}\in B} \rho_{nm}(\mathbf{r})\mathrm{d}\mathbf{r} - \int_{\mathbf{r}\in A} \rho_{nm}(\mathbf{r})\mathrm{d}\mathbf{r} \qquad (6)$$

where $\rho_{nm}(r)$ is the transition density between states m and n, if $m \neq n$, and the state density if $m = n$. Similarly to the FED case, the matrix Δq can be

diagonalized to obtain LE states (such as AB^* and A^*B) with eigenvalue 0, and CT states, such as A^-B^+ or A^+B^-, with eigenvalues 1 or -1, respectively. This is as simple as FED when the adiabatic states are combination of only two diabatic states. The FCD method has already been generalized to treat multiple adiabatic states with the multi-state FCD approach.[24] Our goal is to find the electronic couplings between an excitation localized on either molecule and the CT states. Therefore, we must separate the excited states into four subspaces, namely two CT subspaces (A^-B^+ and A^+B^-), and two LE subspaces (AB^* and A^*B).

Multi-FED-FCD. We start from the already stated definitions of the additional operators Δx and Δq. Except for numerical uncertainties,[24] for CT states like A^-B^+ and A^+B^- Δx should be zero, while $\Delta q = \pm 1$. On the contrary, for LE states such as AB^* and A^*B, Δx equals $+1$ and -1, respectively, and $\Delta q = 0$. We can define the matrix $\mathbb{D} = (\Delta q)^2 - (\Delta x)^2$ with eigenvalues $+1$ and -1, respectively for subspaces of CT and LE states.

The first step of the multi-FCD-FED scheme is to diagonalize $\mathbb{D}$ to separate CT and LE subspaces, similarly to multi-state FCD:[24]

$$\mathbb{U}_1 \mathbb{D} \mathbb{U}_1^\dagger = \mathbb{D}' \tag{7}$$

The same transformation $\mathbb{U}_1$ is applied to Δx and Δq, to obtain $\Delta x'$ and $\Delta q'$. Now, the states can be assigned as either CT or LE depending on the value of $\mathbb{D}'$. $\Delta x'$ and $\Delta q'$ can be each diagonalized within the LE and CT subspaces respectively, so that:

$$\begin{aligned} \mathbb{U}_2 \Delta x' \mathbb{U}_2^\dagger &= \Delta x'' \\ \mathbb{U}_2 \Delta q' \mathbb{U}_2^\dagger &= \Delta q'' \end{aligned} \tag{8}$$

where $\Delta x''$ is diagonal only in the LE block, whereas $\Delta q''$ is diagonal only in the CT block. $\mathbb{U}_2$ is block diagonal and rotates the LE and CT subspaces separately. Within the LE subspace, the diagonal values of $\Delta x''$ can be used to separate AB^* (LE1) states from A^*B (LE2) states. At the same time, $\Delta q''$ can be used to divide CT states in A^-B^+ (CT1) and A^+B^- (CT2). At this point, the four subspaces have been separated. The diagonal electronic Hamiltonian $\mathbb{E}$ can be transformed to this basis as $\mathbb{U}_2\mathbb{U}_1\mathbb{E}\mathbb{U}_1^\dagger\mathbb{U}_2^\dagger = \mathbb{H}''$. As in the multi-state FCD, we require that the Hamiltonian of each subspace is diagonal, *i.e.* that the states of the same subspace are not coupled to each other.[24]

$$\mathbb{U}_3 \begin{pmatrix} \mathbb{H}''_{\mathrm{CT1}} & \mathbb{H}''_{\mathrm{CT1,CT2}} & \mathbb{H}''_{\mathrm{CT1,LE1}} & \mathbb{H}''_{\mathrm{CT1,LE2}} \\ \mathbb{H}''_{\mathrm{CT2,CT1}} & \mathbb{H}''_{\mathrm{CT2}} & \mathbb{H}''_{\mathrm{CT2,LE1}} & \mathbb{H}''_{\mathrm{CT2,LE2}} \\ \mathbb{H}''_{\mathrm{LE1,CT1}} & \mathbb{H}''_{\mathrm{LE1,CT2}} & \mathbb{H}''_{\mathrm{LE1}} & \mathbb{H}''_{\mathrm{LE1,LE2}} \\ \mathbb{H}''_{\mathrm{LE2,CT1}} & \mathbb{H}''_{\mathrm{LH2,CT2}} & \mathbb{H}''_{\mathrm{LE2,LE1}} & \mathbb{H}''_{\mathrm{LE2}} \end{pmatrix} \mathbb{U}_3^\dagger = \begin{pmatrix} \mathcal{E}'''_{\mathrm{CT1}} & \mathbb{H}'''_{\mathrm{CT1,CT2}} & \mathbb{H}'''_{\mathrm{CT1,LE1}} & \mathbb{H}'''_{\mathrm{CT1,LE2}} \\ \mathbb{H}'''_{\mathrm{CT2,CT1}} & \mathcal{E}'''_{\mathrm{CT2}} & \mathbb{H}'''_{\mathrm{CT2,LE1}} & \mathbb{H}'''_{\mathrm{CT2,LE2}} \\ \mathbb{H}'''_{\mathrm{LE1,CT1}} & \mathbb{H}'''_{\mathrm{LE1,CT2}} & \mathcal{E}'''_{\mathrm{LE1}} & \mathbb{H}'''_{\mathrm{LE1,LE2}} \\ \mathbb{H}'''_{\mathrm{LE2,CT1}} & \mathbb{H}'''_{\mathrm{LH2,CT2}} & \mathbb{H}'''_{\mathrm{LE2,LE1}} & \mathcal{E}'''_{\mathrm{LE2}} \end{pmatrix} \tag{9}$$

The unitary matrix $\mathbb{U}_3$ is block diagonal, and each block of $\mathbb{U}_3$ diagonalizes each of the CT1, CT2, LE1, and LE2 blocks of the Hamiltonian. The final Hamiltonian $\mathbb{H}'''$ contains the diabatic energies $\mathcal{E}$ on the diagonal, and the electronic couplings in the off-diagonal blocks. The multi-FED-FCD procedure is schematically outlined in Figure S1 of the Supporting Information.

2.3 Structure and computational details

Structure preparation. A high resolution X-ray structure of *Rps. acidophila* strain 10050 [26] and the *Rps. acidophila* strain 7050 (pdb entry: 1IJD) [11] were used to model B800-B850 and B800-B820 complexes respectively. X-ray structures were cleaned retaining only protein residues, BChls and carotenoids. Missing hydrogen atoms were added with the tleap module of AmberTools [27] considering the titrable residues in their standard protonation states. For both complexes, the N-terminus of the α-apoprotein was treated as a N-carboxymethionine (CXM). Since some residues are missing in the C-terminus apoprotein of structure 1IJD (see Figure S2 in the Supporting Information), both carboxylic groups were capped using methylamine. The position of all hydrogen atoms, the heavy atoms of capping residues, and all other missing atoms was optimized at molecular mechanics (MM) level using Amber14 [27] in combination with the amber ff99SB [28] forcefield for protein residues and GAFF [29] forcefield for cofactors.

BChl optimization. The ground state geometry of each BChl type was optimized at QM/MM level of theory within the ONIOM scheme [30], as implemented in Gaussian16 [31]. The atoms of the BChl ring up to C1 were included in the QM region whereas the other atoms of the phytyl chain were assigned to the MM region and kept frozen during the optimization. The side chain of protein residues directly interacting to the BChl, namely the axially coordinating residues and the hydrogen-bonded residues to the C3-acetyl oxygen of the BChl ring, were included in the QM region and allowed to move. All the other atoms were included in the MM region and kept frozen during the optimization. The QM region was described using DFT at the B3LYP/6-31G(d) level, whereas the MM region was described using the ff99SB forcefield for protein residues and specific forcefields for cofactors [32,33].

Ground-state geometry optimizations of the two adjacent BChl dimers, corresponding to the intra-dimer and inter-dimer BChl pairs (see Figure S3 in the Supporting Information), were also performed. In this case, the conjugated rings of both BChls, as well as their interacting residues, were included in the QM region, as explained before for the optimization scheme of the single BChl.

Excited-state calculations. The excitation energies for each BChl type were calculated with time-dependent DFT (TD-DFT) at the B3LYP/6-31+G(d) level in the QM/MMPol scheme, using the optimized geometries. Electronic couplings were computed at the same level on the unrefined crystal structure, in order to avoid any bias coming from the change in the distance and relative orientations of the BChls. Calculations on the BChl dimers for the CT energies and couplings were performed with the long-range corrected BLYP functional (LC-BLYP) in order to correctly describe the CT states. We used LC-BLYP because the correct asymptotic behaviour of the CT energy can only be reached if the amount of exact exchange is 100% at infinite separation [34]. The range-separation parameter ω was set to 0.195, a value where Q_y energies are rather stable [35].

For CT excitations involving a large density rearrangement, polarizable embedding schemes have to be corrected by a state-specific environmental response [36,37]. We used the first-order corrected Linear Response method to apply the

state-specific correction on the CT energies [38]. Because the state-specific correction only affects energies, it can be applied *a posteriori* only to the CT energies, without influencing the couplings.

In order to be consistent with the B3LYP site energies, we calculated the α^*–CT energy difference from the LC-BLYP calculations and referred these differences to the B3LYP α^* site energies.

3 Results and discussion

The spectroscopic properties of the LH2 complexes are determined by the interactions among the BChls which allow the excited states to delocalize over several pigments, and the interactions between the BChls and the protein in which they are embedded. All excitonic ingredients, as well as possible CT effects, are in fact strongly shaped by the surrounding environment as detailed in the following subsections.

3.1 Q_y Site energies

The Q_y site energy of each BChl is tuned by the local environment of the binding pocket as well as by the longer-range effect of the rest of the protein; both of them contribute to modify the equilibrium geometry of the pigment and modulate its solvatochromic shift. To dissect these two effects, in Table 1 we compare the site energy of an isolated BChl with those of α-BChl and β-BChl calculated using the geometries optimized in the two LH2 complexes. Two sets of data are reported, one calculated by excluding the effect of the environment on the excitation process (VAC) and one calculated including that effect through MMPol. We note that this analysis is limited to α-BChl and β-BChl only, as we assume that the properties of the BChls of the B800 ring are not modified moving from one LH2 complex to the other.

The VAC data for the two complexes, when compared to the isolated BChl, quantify the energy shift due to the changes induced by the environment in the internal geometry of each BChl. For all the different BChls, this shift is rather small (always less than 70 cm^{-1}), still a correlation with a structural datum can be found, namely the C3-acetyl dihedral angle. This angle has been suggested as a possible source for the difference between the two complexes [12]. Indeed, the largest shift (+67 cm^{-1}) is shown in the case of β-BChl of B800-820 where also the largest C3-torsion is found; however, this (small) effect alone cannot explain the observed differences between the two complexes.

The inclusion of the environment in the excitation process through MMPol causes a general shift towards the red for all BChls. In B800-B850 the shifts are very similar for both α-BChl and β-BChl. On the other hand, the shift observed in B800-820 is much lower for the β-BChl than for α-BChl: this can be understood in terms of the change in the hydrogen bond between β-BChl and Tyr, which is lost due to the change of Tyr into Phe in B800-820.

To gain more insight into the contribution of neighboring residues to the red-shift, we repeated the calculation of the excitation energy by selectively "switching off" the protein residues, *i.e.* setting to zero the MMPol charges and polarizabilities

Table 1 Site energies of α-BChl and β-BChl in the two complexes without (VAC) and with (MMPol) including the effect of the environment on the excitation process. Values in parentheses in the VAC column give the shift with respect to the excitation energy of the isolated BChl whereas those in the MMPol column give the shift with respect to the VAC values. All values are in cm^{-1}. The C3-acetyl dihedral angle C4–C3–C3^1–O3^1 (degrees) is also reported.

		E^{VAC}	E^{MMPol}	C3-torsion
Isolated BChl		14832	-	-4
B800-850	α-BChl	14800 (-32)	13978 (-822)	+15
	β-BChl	14853 (+21)	13954 (-899)	-20
B800-820	α-BChl	14859 (+27)	14032 (-800)	-13
	β-BChl	14899 (+67)	14154 (-678)	-31

of each residue. In this analysis we considered every residue that lies within 6 Å of the heavy atoms of the bacteriochlorin ring. We calculated the contribution of a residue by taking the difference between the reference MMPol excitation energy reported in Table 1 and that computed without the selected residue. The contributions are summarized in Figure 2 for α-BChl and β-BChl of B800-850 and B800-820; to have a compact notation the one letter code is used for the residues.

The most important residues contributing to the solvatochromic shift of α-BChl are the hydrogen-bonding residue (Trp(W)45 in B800-850 and Tyr(Y)41 in B800-820), and the close residues of the neighboring β-apoprotein, Ala(A)29 and His(H)30 for both complexes [39, 40, 41]. However, also the neighboring β-BChl on the same unit has a non-negligible contribution. The main differences between B800-850 and B800-820 are found in the α-apoprotein sequence changes. The replacement of Trp(W)45 with Leu(L) leads to a reduced effect; this reduction is however counterbalanced by the replacement of Phe(F)41 with Tyr(Y) which has an opposite effect. The other changed residues, instead, do not significantly contribute to the shift.

For β-BChl, the residues contributing most to the calculated shift are those of the two neighboring α-apoproteins. As expected, the change of Tyr(Y)44 into Phe(F) produces a weaker contribution. Once more, the neighboring BChls also contribute significantly. In particular, the contribution of B800 BChl is greater in the B800-820 complex than in B800-850; the reason for this difference may lie in the position of the the phytyl chain of one of the B800-BChls, which is in van der Waals contact with ring I and IV of the α-BChl's macrocycle in B800-820 but not in the B800-850 structure here used (See Figure S4 in the Supporting Information).

We conclude that this first analysis shows a limited effect of the different hydrogen-bond network in distinguishing β-BChl in the B800-850 and B800-820 complexes: a net blue-shift of only 150–200 cm^{-1} is in fact found in the B800-820 complex. To further validate this finding, we investigated the possible role of non-classical effects by repeating the calculations with the inclusion of the hydrogen-bonded residues in the QM region (QM-Large/MMPol). The results (Table S1 of the Supporting Information) show negligible difference between the QM-Large/MMPol and QM/MMPol calculations, confirming that the classical MMPol model is able to correctly describe the hydrogen-bonding effects.

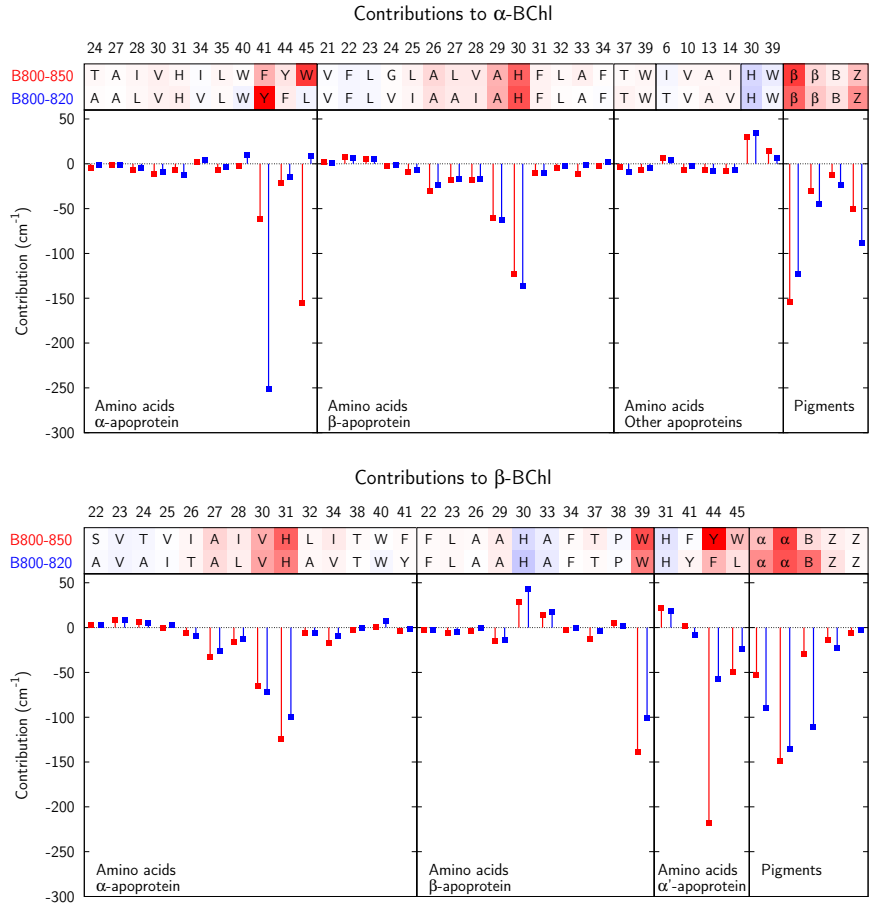

Fig. 2 Contributions to the Q_y transition obtained by switching off the MMPol effect of single aminoacids. Top panel: contributions to the transition of α-BChl. Bottom panel: contributions to the transition of β-BChl. We denote by α-apoprotein and β-apoprotein those peptide chains that belong to the same $\alpha\beta$-apoprotein pair of the considered Bchl, whereas α'-apoprotein refers to the α-apoprotein of the neighboring $\alpha\beta$-apoprotein. Amino acids are displayed using the one letter code, the two close-by BChls in the ring are displayed using "α" and "β" whereas "B" refers to the closest B800-BChl; the close-by carotenoids are displayed using "Z".

3.2 Q_y–Q_y Couplings

The exciton structure of the two LH2 complexes is mainly determined by the nearest-neighbour inter- and intra-dimer couplings in the B850 and B820 ring, respectively. The calculated values are reported in Table S2 of the Supporting Information. The B820 ring presents an inter-dimer coupling ($V^1_{\alpha\beta}$) significantly smaller than in B850, whereas the intra-dimer coupling ($V^2_{\alpha\beta}$) is slightly larger. All other couplings are instead very similar in the two complexes. We note that the B850 couplings are somewhat smaller than the ones reported in our previous work

[16], which however was based on a different crystal structure and used a different DFT functional.

To better understand the origin of these differences, it is important to dissect the direct Culomb coupling and the effect of the environment. In QM/MMPol, the atomistic description of the environment allows the specific effects of each residue to be properly accounted for: this direct contribution is represented by the second term of eq. 3. The analysis of this term can be eased by introducing an effective dielectric constant, which is specific to each (ij) pair of pigments:[16, 42]

$$\varepsilon_{ij}^{\text{eff}} = \frac{V_{ij}^{\text{Coul}}}{V_{ij}^{\text{Coul}} + V_{ij}^{\text{MMPol}}} \tag{10}$$

The calculated values of $\varepsilon_{ij}^{\text{eff}}$ present a similar behavior in the two complexes, with the values of ε^{eff} being very different for two nearest-neighbour couplings (See Table S2 in the Supporting Information). For the intra-dimer coupling, ε_{eff} is 1.4, whereas for the inter-dimer coupling it is close to 1, that is, there is virtually no screening due to the environment. To investigate the origin of this difference, we dissected the MMPol term in the coupling into contributions from the single residues [42].

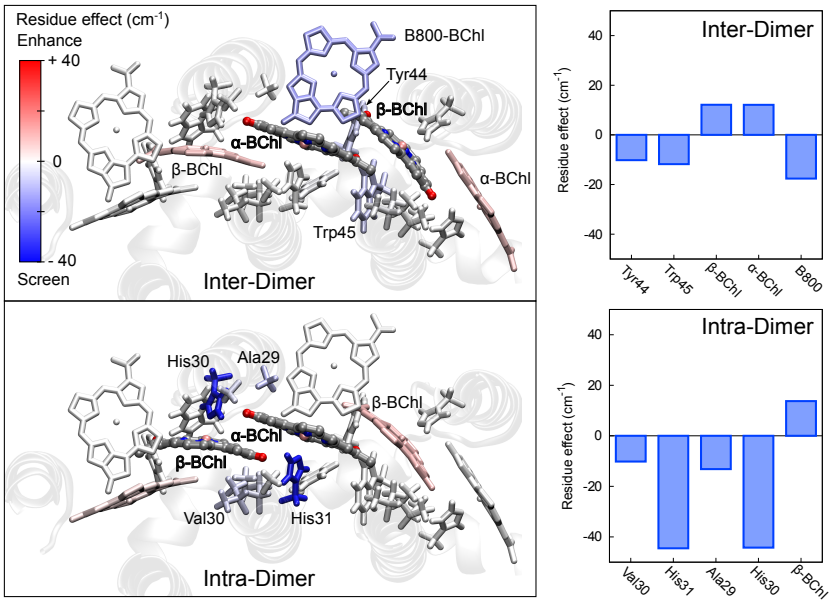

Fig. 3 Representation of residue contributions to the nearest-neighbour inter-dimer (top) and intra-dimer (bottom) electronic couplings in B800-850. Blue and red colours correspond respectively to a reduction and an enhancement of the coupling. QM BChls are enlightened using different colors.

As shown in Figure 3, in the intra-dimer coupling, the axial histidines (His) are responsible for a large part of the screening, while the neighboring α and β BChls give a small enhancement. The axial His screens the coupling in the intra-dimer

$\alpha\beta$ BChl pair, but not in the inter-dimer analogue, because in the former the His position allows a strong polarization interaction with both the coupled BChls. In the inter-dimer case, moreover, the coupling is enhanced by the neighboring α and β BChls, and this finally results in a very low net screening.

3.3 Exciton model

The calculated site energies and couplings were finally combined in the excitonic Hamiltonian (1) to obtain the excitonic states of the B800-B850 and B800-820 complexes, among which only few are bright due to the high structural symmetry. In particular, the orientation of the transition dipole that characterizes the Q_y excitation, when combined with the relative orientation of the BChls in the two rings, leads to a concentration of most of the excitonic dipole strength in two degenerate states (also denoted as $k = \pm 1$) of each ring [2,14], resulting in the two bands of the absorption spectrum (see Table S3 in the Supporting Information).

From the site energies and couplings discussed in the previous subsections, we obtain that the bright $k = \pm 1$ states of B820 are blue shifted by $\sim$150 cm^{-1} with respect to the same states of B850. This blue-shift is much smaller than what is experimentally observed ($\sim$510 cm^{-1}) [43].

To investigate this discrepancy, we analysed some artificial models obtained by successively substituting the B800-850 excitonic parameters with those obtained from the B800-820 complex (see Figure 4). Three different parameters have been considered: site energies of α-BChl, site energies of β-BChl, and couplings. As expected, by changing the α-BChl site energies, we get a very small shift ($\sim$20 cm^{-1}) of the bright excitonic $k = \pm 1$ state. The same result is obtained if we only change the couplings. In contrast, a much larger effect ($\sim$120 cm^{-1}) is found when we change the β-BChl site energies: this can be seen as a quantification of the loss of the hydrogen bond. We also note that the effects of the three changes are additive.

As a last analysis, we considered another spectroscopic parameter, the exciton width W, which is defined as the energy difference between the lowest ($k = \pm 1$) and the highest pair of degenerate states ($k = \pm 8$) of the B850 or B820 band: its

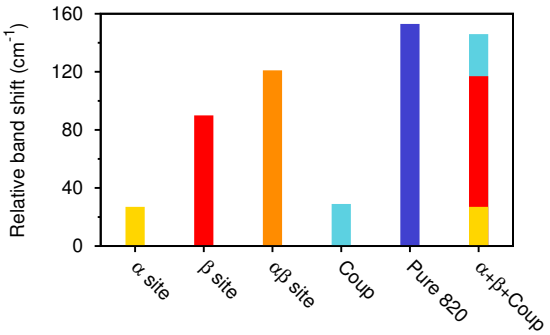

Fig. 4 Excitonic band energies (relative to B850) obtained by substituting B800-850 parameters (site energies of α-BChl, site energies of β-BChl, and couplings) with the ones computed on the B800-820 complex. The last bar is the sum of α, β and Coup shifts.

value was measured in fluorescence excitation anisotropy experiments [14,44]. The exciton width is mostly determined by the excitonic couplings within the ring, with the main contribution coming from the coupling of neighboring α and β BChls. Moving from B850-800 to B820-800 W is reduced by 46 cm^{-1}. This reduction is in line with the experiments (152 cm^{-1}) [44,14], but it is underestimated.

Summarizing the results reported so far, we can say that the effects due to the different structure and the different hydrogen-bonding network are not sufficient to fully recover the observed blue shift of the B800-820 complex with respect to B800-850. In the next Section, we will assess the effect of charge transfer (CT) excited states between BChls on the exciton structure of the two forms of LH2.

3.4 Effect of Charge Transfer States

To estimate the effect of CT states within the B850 (B820) ring, we selected the two $\alpha\beta$ BChl pairs, which are shown in Figure 5.

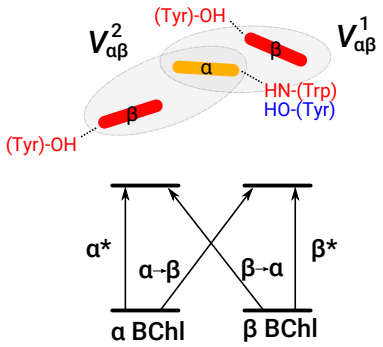

Fig. 5 (top) Schematic representation of the inter-dimer ($V^1_{\alpha\beta}$) and intra-dimer ($V^2_{\alpha\beta}$) BChl pairs. Hydrogen bonding residues are specified, in red for B800-B850, in blue for B800-B820 LH2. (bottom) Representation of the four possible excited states in each BChl pair.

The couplings calculated with the diabatization scheme presented in the Methods section are reported in Table 2 for both dimers in B800-850 and B800-820. The couplings refer to both Q_y–Q_y , and CT–Q_y states.

Table 2 Couplings among the four states of each $\alpha\beta$ dimer described in Figure 5, for B800-850 and for B800-820. All values are in cm^{-1}.

States		B800-850		B800-820	
		Intra-dimer	Inter-dimer	Intra-dimer	Inter-dimer
α^*	β^*	287	306	271	270
α^*	$\alpha \rightarrow \beta$	-579	-376	-480	-15
α^*	$\beta \rightarrow \alpha$	-369	-341	-309	-211
β^*	$\alpha \rightarrow \beta$	371	309	294	161
β^*	$\beta \rightarrow \alpha$	613	428	517	123

For B800-850, both dimers present fairly large couplings between Q_y and CT states which reduce by 20–40% passing to B800-820. In particular, the inter-dimer couplings drop to less than 200 cm^{-1}. This reduced interaction with CT states is expected to affect the energies of the bright excitonic states.

The CT states (which lie 5000–6000 cm^{-1} above the Q_y states) were added to the excitonic Hamiltonian as in eq. (2); diagonalization of the new extended Hamiltonian yields exciton states with lower energies due to their mixing with CT states (See Table S4 in the Supporting Information). In particular, the Q_y–CT couplings combine in such a way that the lowest exciton states are more red-shifted by the mixing, while the highest states are virtually unaffected (See Figure S5 in the Supporting Information). The net effect is a significant red-shift of the B850/B820 bright $k = \pm 1$ states, and an increase in the energy difference between the $k = \pm 1$ and $k = \pm 8$ states. The exciton width in the B850 ring thus becomes 1335 cm^{-1}, while the in the B820 ring it becomes 1097 cm^{-1}, closer to the experimental values of 1442 cm^{-1} and 1290 cm^{-1}, respectively [14,44].

Since in the B800-820 complex the couplings to CT states are smaller, the lowest exciton states are less red-shifted by the mixing. Thus, the difference in the energy of the $k = \pm 1$ state between the two LH2 complexes becomes ~300 cm^{-1} (see Figure 6). The CT states thus modulate the energy of the bright states by an amount that equals the combined effect shown in the previous section of the different site energies and excitonic couplings.

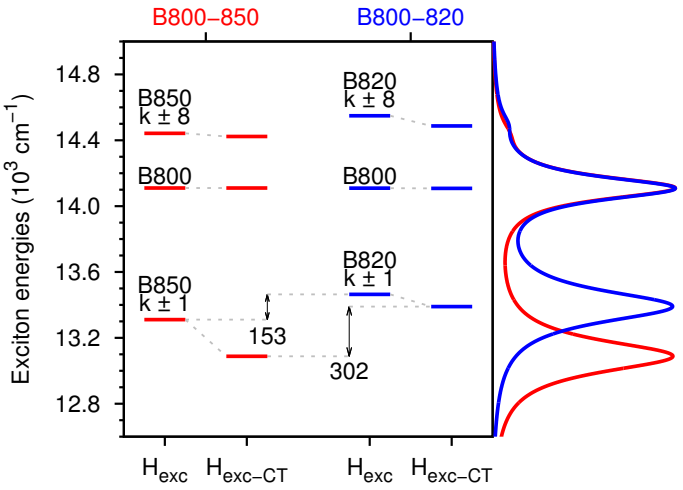

Fig. 6 CT effect on the excitonic states of the complexes. The arrows show the B820-B850 energy difference (cm^{-1}) before and after the addition of CT states.

As the couplings between Q_y and CT states are determined by wavefunction overlap between α and β BChl, they strongly depend on the separation between the two moieties, and thus we can expect that their magnitude will fluctuate due to thermal motions. Moreover, we can also expect that the lack of a hydrogen bond in B820β allows larger fluctuations in the $\alpha\beta$ interpigment distance, which

reflect in larger coupling fluctuations. As the fluctuations of Q_y-CT couplings will contribute to the broadening of the band, larger fluctuations in the couplings of the B800-820 complex could also explain the observed larger energetic disorder within the B820 ring compared to the B850 [2, 9, 45].

Even though the inclusion of CT states significantly improves the agreement with experiments, the predicted blue-shift is still quantitatively too small. We can expect that geometrical fluctuations will affect the differences between the two forms of LH2, therefore a dynamical description of LH2, e.g. through a molecular dynamics simulation, would be fundamental to achieve a more quantitative agreement with the experiment.

4 Conclusions

A multiscale model, which combines a quantum chemical description of the pigments with a classical but atomistic description of the environment, has been employed in this study to understand the molecular origin of the spectral differences between the B800-850 and B800-820 forms of LH2. To achieve a better description of the mutual interactions between the QM pigments and the classical protein, a polarizable model has been introduced for the latter, thus allowing a proper evaluation of its effects on both site energies and couplings.

We have first analyzed the effect of the changing in the hydrogen bond between the C3-acetyl group and the protein residues in the two forms. The analysis of the Q_y excitation energies of BChls showed that the rotation of the C3-acetyl group due to the change of hydrogen bond in the α-BChl of B800-820, has a small effect (less than 60 cm^{-1}) [13]. In contrast, the loss of the hydrogen-bond due to the change of Tyr to Phe induces a much larger solvatochromic shift of β-BChl. No significant differences are instead found in the electronic couplings of the two complexes. In both cases, the nearest-neighbor couplings are screened differently in the intra- and inter- dimer BChl pair, owing to the different local environment, and in particular to the position of His residues, which lie between the BChls of the intra-dimer pair, but are external to the inter-dimer. The different site-energies calculated for β-BChl in the two complexes are responsible for a net blue-shift of about 150 cm^{-1} of the first bright exciton state of B800-820. This shift is in line with the experimental evidence but it is not enough to quantitatively reproduce the spectral change [41].

The agreement between simulation and experiment is improved when charge transfer states between adjacent BChls are included in the excitonic Hamiltonian. The coupling between CT and Q_y states influences the exciton structure of the complex lowering the energy of the first bright exciton state, which gives rise to the longest wavelength band in the absorption spectrum. The structural differences between the two complexes provide a 20–40% reduction of the CT–Q_y coupling values in B800-820 with respect to B800-850. This reduction results in a smaller exciton width for the B820 ring with respect to the B850, and a net blue-shift of $\sim$300 cm^{-1} of the lowest exciton bright state in B800-820. These results suggest a new possible explanation of the observed blue-shift in the B800-820 form of LH2 where the different hydrogen bond network not only affects the Q_y transitions of the different BChls but it also indirectly affects the role of CT states.

If this is the case, a new perspective is possible for giving a rationalization of the many different spectroscopic forms of LH2 found in purple bacteria. As for most of them, there are no high resolution structures available, what is left is information from the sequence of their LH2 apoproteins and spectroscopic data. Further theoretical studies, also including the dynamics of the pigments and the environment, are thus required to provide a better understanding of what to look for in the primary sequence data to allow an accurate prediction of the spectroscopic form.

Acknowledgements The authors are grateful to Dr. Aleksander W. Roszak for having provided the high-resolution X-ray structure of B800-850 complex. ATG and RJC gratefully acknowledge funding from the Photosynthetic Antenna Research Center, an Energy Frontier Research Center funded by the DOE, Office of Science, Office of Basic Energy Sciences under Award Number DE-SC 0001035.

References

1. B. Robert, R.J. Cogdell, R. van Grondelle, in *Light-Harvesting Antennas in Photosynthesis*, ed. by B.R. Green, W.W. Parson (Springer Netherlands, Dordrecht, 2003), pp. 169–194
2. R.J. Cogdell, A. Gall, J. Köhler, Q. Rev. Biophys. **39**(3), 227 (2006). DOI 10.1017/S0033583506004434
3. J. Aagaard, W.R. Sistrom, Photochem. Photobiol. **15**(2), 209 (1972). DOI 10.1111/j.1751-1097.1972.tb06240.x
4. S. Kaplan, in *The Photosynthetic Bacteria*, ed. by R.K. Clayton, W.R. Sistrom (Plenum Press, New York and London, 1978), pp. 809–839
5. R.J. Cogdell, I. Durant, J. Valentine, J. Lindsay, K. Schmidt, Biochim. Biophys. Acta - Bioenerg. **722**(3), 427 (1983). DOI 10.1016/0005-2728(83)90058-0
6. A.T. Gardiner, R.J. Cogdell, S. Takaichi, Photosynth. Res. **38**(2), 159 (1993)
7. S.L. Henry, R.J. Cogdell, Adv. Bot. Res. **66**, 205 (2013). DOI 10.1016/B978-0-12-397923-0.00007-2
8. H. Zuber, R.J. Cogdell, in *Anoxygenic Photosynthetic Bacteria*, ed. by R.E. Blankenship, M.T. Madigan, C.E. Bauer (Springer Netherlands, Dordrecht, 1995), pp. 315–348
9. G.J.S. Fowler, R.W. Visschers, G.G. Grief, R. van Grondelle, C.N. Hunter, Nature **355**, 848 (1992). DOI 10.1038/355848a0
10. G.J. Fowler, G.D. Sockalingum, B. Robert, C.N. Hunter, Biochem. J. **299**, 695 (1994)
11. K. McLuskey, S.M. Prince, R.J. Cogdell, N.W. Isaacs, Biochemistry **40**(30), 8783 (2001)
12. E. Gudowska-Nowak, M.D. Newton, J. Fajer, J. Phys. Chem. **94**(15), 5795 (1990)
13. J. Chmeliov, E. Songaila, O. Rancova, A. Gall, B. Robert, D. Abramavicius, L. Valkunas, J. Phys. Chem. B **117**(38), 11058 (2013). DOI 10.1021/jp400239z
14. A. Freiberg, K. Timpmann, G. Trinkunas, Chem. Phys. Lett. **500**(1-3), 111 (2010). DOI 10.1016/j.cplett.2010.09.084
15. M. Ferretti, R. Hendrikx, E. Romero, J. Southall, R.J. Cogdell, V.I. Novoderezhkin, G.D. Scholes, R. van Grondelle, Sci. Rep. **6**(November 2015), 20834 (2016). DOI 10.1038/srep20834
16. L. Cupellini, S. Jurinovich, M. Campetella, S. Caprasecca, C.A. Guido, S.M. Kelly, A.T. Gardiner, R. Cogdell, B. Mennucci, J. Phys. Chem. B **120**(44), 11348 (2016). DOI 10.1021/acs.jpcb.6b06585
17. X. Li, R.M. Parrish, F. Liu, S.I.L. Kokkila Schumacher, T.J. Martínez, J. Chem. Theory Comput. **13**(8), 3493 (2017). DOI 10.1021/acs.jctc.7b00171
18. C. Curutchet, B. Mennucci, Chem. Rev. **117**(2), 294 (2017)
19. C. Curutchet, A. Muñoz Losa, S. Monti, J. Kongsted, G.D. Scholes, B. Mennucci, J. Chem. Theory Comput. **5**, 1838 (2009). DOI 10.1021/ct9001366
20. S. Jurinovich, L. Cupellini, C.A. Guido, B. Mennucci, J. Comput. Chem. **39**(5), 279 (2018). DOI 10.1002/jcc.25118
21. C. Curutchet, G.D. Scholes, B. Mennucci, R. Cammi, J. Phys. Chem. B **111**(46), 13253 (2007). DOI 10.1021/jp075411h

22. M.F. Iozzi, B. Mennucci, J. Tomasi, R. Cammi, J. Chem. Phys. **120**(15), 7029 (2004). DOI 10.1063/1.1669389
23. A.A. Voityuk, N. Rösch, J. Chem. Phys. **117**(12), 5607 (2002). DOI 10.1063/1.1502255
24. C.H. Yang, C.P. Hsu, J. Chem. Phys. **139**(15), 154104 (2013). DOI 10.1063/1.4824906
25. C.p. Hsu, Z.Q. You, H.C. Chen, J. Phys. Chem. C **112**(4), 1204 (2008). DOI 10.1021/jp076512i
26. The high-resolution structure was provided by Dr. Aleksander W. Roszak, University of Glasgow, unpublished results
27. D.A. Case, V. Babin, J.T. Berryman, R.M. Betz, Q. Cai, D.S. Cerutti, T.E. Cheatham, T.A. Darden, R.E. Duke, H. Gohlke, A.W. Goetz, S. Gusarov, N. Homeyer, P. Janowski, J. Kaus, I. Kolossváry, A. Kovalenko, T.S. Lee, S. LeGrand, T. Luchko, R. Luo, B. Madej, K.M. Merz, F. Paesani, D.R. Roe, A. Roitberg, C. Sagui, R. Salomon-Ferrer, G. Seabra, C.L. Simmerling, W. Smith, J. Swails, Walker, J. Wang, R.M. Wolf, X. Wu, P.A. Kollman, *Amber 14*. University of California, San Francisco (2014)
28. V. Hornak, R. Abel, A. Okur, B. Strockbine, A. Roitberg, C. Simmerling, Proteins Struct. Funct. Bioinforma. **65**(3), 712 (2006). DOI 10.1002/prot.21123
29. J. Wang, R.M. Wolf, J.W. Caldwell, P.A. Kollman, D.A. Case, Journal of Computational Chemistry **25**(9), 1157 (2004). DOI 10.1002/jcc.20035
30. L.W. Chung, H. Hirao, X. Li, K. Morokuma, Wiley Interdisciplinary Reviews: Computational Molecular Science **2**(2), 327 (2011)
31. M.J. Frisch, G.W. Trucks, H.B. Schlegel, G.E. Scuseria, M.A. Robb, J.R. Cheeseman, G. Scalmani, V. Barone, G.A. Petersson, H. Nakatsuji, X. Li, M. Caricato, A.V. Marenich, J. Bloino, B.G. Janesko, R. Gomperts, B. Mennucci, H.P. Hratchian, J.V. Ortiz, A.F. Izmaylov, J.L. Sonnenberg, D. Williams-Young, F. Ding, F. Lipparini, F. Egidi, J. Goings, B. Peng, A. Petrone, T. Henderson, D. Ranasinghe, V.G. Zakrzewski, J. Gao, N. Rega, G. Zheng, W. Liang, M. Hada, M. Ehara, K. Toyota, R. Fukuda, J. Hasegawa, M. Ishida, T. Nakajima, Y. Honda, O. Kitao, H. Nakai, T. Vreven, K. Throssell, J.A. Montgomery, Jr., J.E. Peralta, F. Ogliaro, M.J. Bearpark, J.J. Heyd, E.N. Brothers, K.N. Kudin, V.N. Staroverov, T.A. Keith, R. Kobayashi, J. Normand, K. Raghavachari, A.P. Rendell, J.C. Burant, S.S. Iyengar, J. Tomasi, M. Cossi, J.M. Millam, M. Klene, C. Adamo, R. Cammi, J.W. Ochterski, R.L. Martin, K. Morokuma, O. Farkas, J.B. Foresman, D.J. Fox. Gaussian 16 Revision A.03 (2016). Gaussian Inc. Wallingford CT
32. M. Ceccarelli, P. Procacci, M. Marchi, J. Comput. Chem. **24**(2), 129 (2003). DOI 10.1002/jcc.10198
33. I. Guarnetti-Prandi, L. Viani, O. Andreussi, B. Mennucci, J. Comp. Chem. **37**(11), 981 (2016). DOI 10.1002/jcc.24286
34. A. Dreuw, J.L. Weisman, M. Head-Gordon, J. Chem. Phys. **119**(6), 2943 (2003). DOI 10.1063/1.1590951
35. M. Higashi, T. Kosugi, S. Hayashi, S. Saito, J. Phys. Chem. B **118**(37), 10906 (2014). DOI 10.1021/jp507259g
36. C.A. Guido, D. Jacquemin, C. Adamo, B. Mennucci, J. Chem. Theory Comput. **11**(12), 5782 (2015). DOI 10.1021/acs.jctc.5b00679
37. R. Guareschi, O. Valsson, C. Curutchet, B. Mennucci, C. Filippi, J. Phys. Chem. Lett. **7**(22), 4547 (2016). DOI 10.1021/acs.jpclett.6b02043
38. M. Caricato, B. Mennucci, J. Tomasi, F. Ingrosso, R. Cammi, S. Corni, G. Scalmani, J. Chem. Phys. **124**(12), 124520 (2006). DOI 10.1063/1.2183309
39. G.D. Scholes, I.R. Gould, R.J. Cogdell, G.R. Fleming, J. Phys. Chem. B **103**(13), 2543 (1999)
40. S. Jang, E. Rivera, D. Montemayor, J. Phys. Chem. Lett. **6**(6), 928 (2015)
41. A. Anda, L. De Vico, T. Hansen, J. Phys. Chem. B **121**(22), 5499 (2017). DOI 10.1021/acs.jpcb.7b02071
42. C. Curutchet, J. Kongsted, A. Muñoz-Losa, H. Hossein-Nejad, G.D. Scholes, B. Mennucci, J. Am. Chem. Soc. **133**(9), 3078 (2011)
43. N.M. Magdaong, A.M. LaFountain, J.A. Greco, A.T. Gardiner, A.M. Carey, R.J. Cogdell, G.N. Gibson, R.R. Birge, H.A. Frank, J. Phys. Chem. B **118**(38), 11172 (2014)
44. M. Pajusalu, M. Rätsep, G. Trinkunas, A. Freiberg, ChemPhysChem **12**(3), 634 (2011). DOI 10.1002/cphc.201000913
45. W. de Ruijter, J. Segura, R. Cogdell, A. Gardiner, S. Oellerich, T. Aartsma, Chem. Phys. **341**(1-3), 320 (2007)